Numerical Simulation of Turbulent Reacting Flows in Combustion Chambers

X.S. Bai and L. Fuchs

Dept. of Gasdynamics, Royal Institute of Technology

S-100 44 Stockholm, Sweden

Abstract

The numerical computation of turbulent reacting flows in combustion chambers of a gas turbine engine are carried out. The Reynolds averaged Navier–Stokes equations and the two–equation k–ε model together with either premixed flame or diffusion flame reaction models are used. The numerical scheme employed here is finite difference based, together with Multi–Grid method and Local grid refinement technique. The mathematical models and numerical method are applied to simulating the main burners and afterburners of a gas turbine engine.

1. Introduction

An important aspect for aircraft engine design is the adequate prediction of the reacting flow fields in combustion chambers. The velocity and temperature fields and detailed knowledge of many other factors that would influence the performance of engines directly guide the modification of engine components. Frequently experimental study and previous experience are the main reference sources for designing new engines. This approach has been proved to be reliable though by no means economical and optimal. One of the barriers for using theoretical analysis tools in design is the lack of adequate analytical methods since the governing equations of turbulent reacting flows are highly non–linear and exact solution of such flow problem is not available. The objective of this paper is to exhibit our effort in solving numerically turbulent reacting flow problems in engine combustion chambers.

The governing equations for turbulent reacting flows are considered to be the Navier–Stokes equation provided with chemical kinetics [1]. However direct numerical simulation of such equations in high Reynolds number turbulent regimes for complex geometry problem like engine combustors is not possible due to the limitation of computer capacity. Instead we use modelling techniques, that is, using the Reynolds averaged Navier–Stokes equation together with a two–equation turbulent model [2,3,4] and simplified chemical models [5–8]. Earlier applications of these mathematical models have proved to be adequate both for turbulent isothermal flows [9,10] and turbulent reacting flows [11–13].

The numerical methods that we used here include both finite difference discretization of the governing equations. The system of equations is solved by a Multi-

Grid method (MG) with possible local grid refinement technique. The MG method generally accelerates the convergence of iteration process [14] and local grid refinement utilizes a given number of degree of freedom in an efficient way [15]. The application of the numerical methods to simulating reacting flows in the gas turbine engine combustion chamber gives reasonable prediction of the flame structure and fuel burning efficiency variations with different burner structure arrangements. Another example that has been considered is the blockage ratio and the shape of bluff body flame holders in afterburners. These calculations illustrate the potential capacity of numerical computations in aircraft engine design.

2. Mathematical Models

For high Reynolds number turbulent reacting flows the Reynolds averaged Navier–Stokes equation and continuity equation are given by:

$$\frac{\partial \varrho}{\partial t} + \frac{\partial \varrho U_j}{\partial x_j} = 0 \tag{1}$$

$$\frac{\partial \varrho U_i}{\partial t} + \frac{\partial \varrho U_i U_j}{\partial x_j} = -\frac{\partial p}{\partial x_i} + \frac{\partial \tau_{ij}}{\partial x_j}$$
$$+ \frac{\partial}{\partial x_j}[\mu(\frac{\partial U_i}{\partial x_j} + \frac{\partial U_j}{\partial x_i} - \frac{2}{3}\delta_{ij}\frac{\partial U_k}{\partial x_k})] \tag{2}$$

Where ρ, U_i, p are density, cartesian components of the velocity vector and pressure in Favre averaged sense. μ is viscosity, $\tau_{ij} = -\overline{\varrho u_i u_j}$ is Reynolds stress tensor, which is modeled as [8]:

$$\overline{\varrho u_i u_j} = \frac{2}{3}\delta ij(\varrho k + \mu_t \frac{\partial U_k}{\partial x_k}) - \mu_t(\frac{\partial U_i}{\partial x_j} + \frac{\partial U_j}{\partial x_i})$$

k is the turbulent kinetic energy μ_t is the turbulent eddy viscosity computed from k and ε (the dissipation rate of k) model:

$$\mu_t = \varrho C_\mu \frac{k^2}{\varepsilon} \tag{3}$$

$$\frac{\partial \varrho k}{\partial t} + \frac{\partial \varrho k U_j}{\partial x_j} = \frac{\partial}{\partial x_j}[(\mu + \frac{\mu_t}{\sigma_k})\frac{\partial k}{\partial x_j}] + S_k \tag{4}$$

$$\frac{\partial \varrho \epsilon}{\partial t} + \frac{\partial \varrho \epsilon U_j}{\partial x_j} = \frac{\partial}{\partial x_j}[(\mu + \frac{\mu_t}{\sigma_\epsilon})\frac{\partial \epsilon}{\partial x_j}] + S_\epsilon \quad (5)$$

$$S_k = \tau_{ij}\frac{\partial U_j}{\partial x_j} - \varrho \epsilon - \frac{\mu_t}{\varrho^2}\frac{\partial \varrho}{\partial x_j}\frac{\partial p}{\partial x_j}$$

$$S_\epsilon = C_1 \frac{\epsilon}{k}[\tau_{ij}\frac{\partial U_j}{\partial x_j} - \frac{\mu_t}{\varrho^2}\frac{\partial \varrho}{\partial x_j}\frac{\partial p}{\partial x_j}] - C_2\varrho\frac{\epsilon^2}{k}$$

In the relations above, density (and viscosity) is linked either with pressure or temperature (T) through equation of state. The temperature is obtained from energy conservation equation:

$$\frac{\partial \varrho h}{\partial t} + \frac{\partial \varrho h U_j}{\partial x_j} - \frac{\partial p}{\partial t} = \frac{\partial}{\partial x_j}[(\frac{\mu + \mu_t}{\sigma_h})\frac{\partial h}{\partial x_j}] + H_\alpha^0 R_\alpha \quad (6)$$

Where H_α^0 is energy formation constant, $h = \int_{T_0}^{T} C_p dT$ is enthalpy. Density (and viscosity) is also linked with mass fractions of chemical species (m_α). The equations for mass fractions are:

$$\frac{\partial \varrho m_\alpha}{\partial t} + \frac{\partial \varrho m_\alpha U_j}{\partial x_j} = \frac{\partial}{\partial x_j}[(\frac{\mu + \mu_t}{\sigma_m})\frac{\partial m_\alpha}{\partial x_j}] - R_\alpha \quad (7)$$

In equations (3)–(7), C_μ, C_1, C_2, σ_k, σ_ϵ, σ_h, σ_m are model constants. R_α is the chemical reaction rate of specie α, where α is either fuel, oxygen, nitrogen, or carbon dioxide etc. In our computation we assume that the reaction is fast and consists of a single step:

$$Fuel + Oxygen \rightarrow Products \quad (8)$$
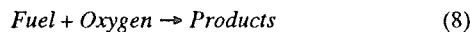
Two distinct reaction rate models have been used:

A. Premixed flame model: The model used here was developed by Magnussen and Hjertager [7], which is based on the eddy dissipation concept: The reaction rate is limited by turbulent mixing rate. For situations with low temperature no reaction may take place. The effective reaction rate in the calculation is:

$$R_{fuel} = \min[A\varrho \min(m_{fuel}, \frac{m_{oxygen}}{r}, B\frac{m_{products}}{1+r})\frac{\epsilon}{k},$$

$$C\varrho^a m_{fuel}^b m_{oxygen}^c \exp(-\frac{E}{RT})] \quad (9)$$

$$R_{oxygen} = rR_{fuel} \quad (10)$$

Where A, B, C, a, b, c, E, R are model constants, r is the stoichiometric constant of reaction.

B. Diffusion flame model: For situations where fuel and air enter the combustion chamber in different streams, we assume that the combustion time scale is much shorter than the characteristic scale of the flow so that the fuel and air react immediately when they are meeting. Assuming chemical reaction is in chemical equilibrium, equation (10) is valid, we can introduce a new variable – mixture fraction (f): $f = (\phi - \phi_{\text{at oxygen inlet}})/C$, $\phi = m_{fuel} - m_{oxygen}/r$. C is constant for normalizing f, so that f is in [0,1]. Let f_s denotes the value of f at point where $\phi = 0$. If $f < f_s$, $m_{fuel} = 0$, if $f > f_s$ then $m_{oxygen} = 0$. In each case the undetermined oxygen or fuel mass fraction can be computed through definition of f and ϕ.

For both models A and B, the mass fractions of products can be computed through the reaction formulation (8) and $\Sigma m_\alpha = 1$.

The model constants used in the computation are as in reference [12,13].

3. Numerical Methods

The system of governing equations is approximated by finite differences. Second order central differences are used to approximate the diffusive terms. Hybrid (central/upwind) differences are used to approximate convective terms, depending on the local Peclet number. The discrete system of equation is solved by a Multi-Grid (MG) method [14]. The smoother consists of a sequence of sweeps (pointwise relaxation) on each equation. When the continuity equation is updated at a given cell, the velocity and pressure are updated simultaneously. The transfer to coarse grids is done by volume averaging and corrections are interpolated to fine grids by trilinear interpolations.
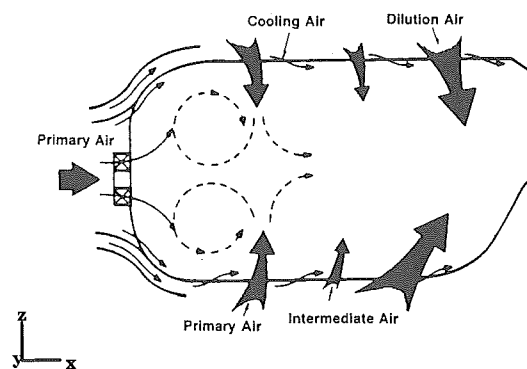

Figure 1. Illustration of the main chamber of a gas turbine engine

In order to get improved resolution at near wall regions, a local grid refinement technique is used [15]. These local gird refinements are either isotropic (i.e. the same refinement in each direction), or non–isotropic (no refinement in directions parallel to the solid wall). The boundary conditions on locally refined grids are either

given (at physical boundaries) or derived from the values on the next coarser grid (at internal boundaries).

4. Numerical Results

4.1 The combustion in the main chamber

Figure 1 shows an illustration of the main chamber of a gas turbine engine. The fuel is injected in the dome surrounded by swirling primary air. Another stream of primary air is supplied through the first row of liner air holes, resulting the full mixing with the incoming fuel. To complete the combustion process and reduce the high temperature of the outlet hot gas the intermediate air and dilution air are introduced through the second row and rear row of the liner.
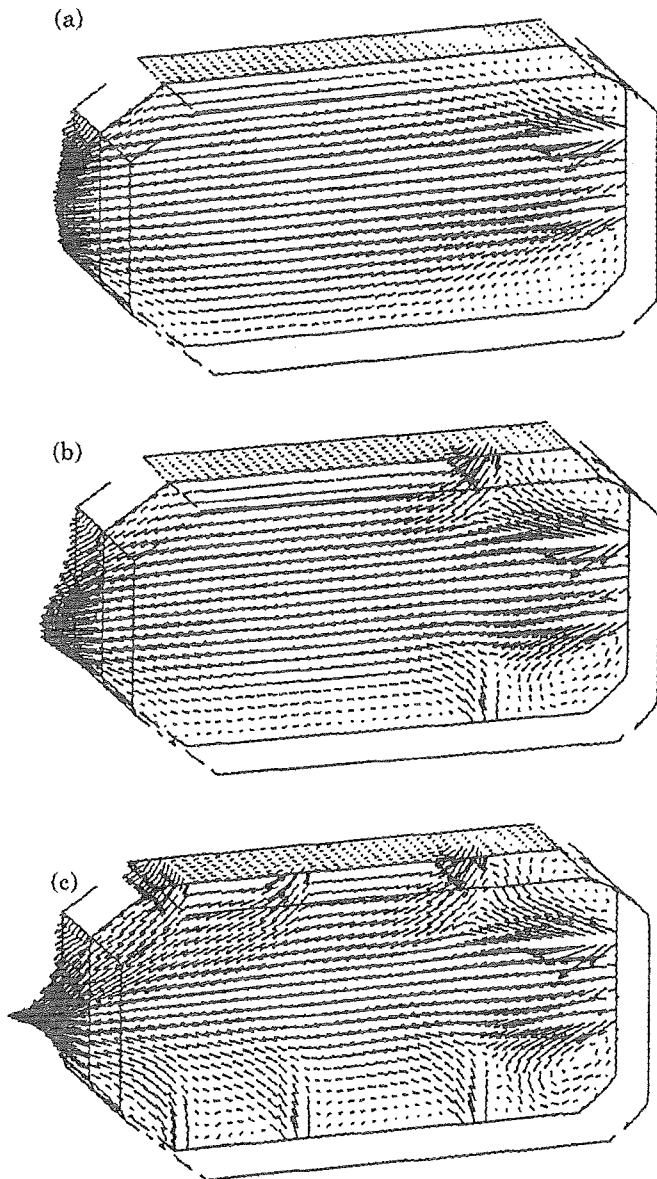
(a)

(b)

(c)

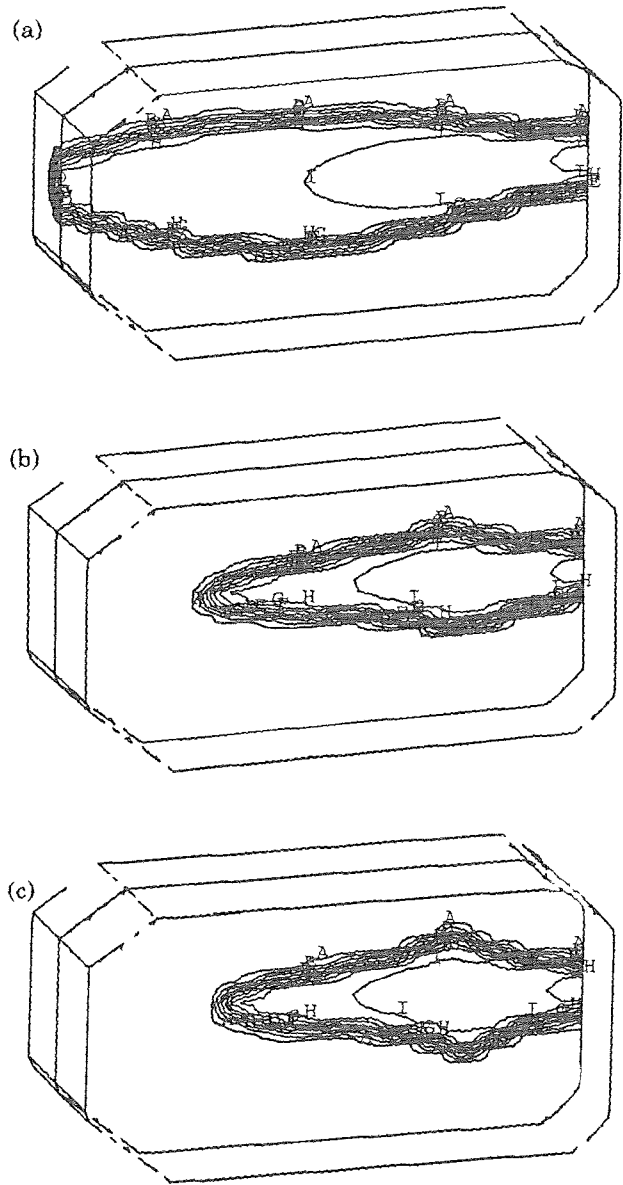Figure 2. Calculated velocity vector field of main chambers: (a)–case 1; (b)–case 2; (c)–case 3.

(a)

(b)

(c)

Figure 3. Calculated mass fraction distribution in the main chambers: A– 10^{-9}, B– 10^{-8}, C– 10^{-7}, D– 10^{-6}, E– 10^{-5}, F– 10^{-4}, G– 10^{-3}, H– 10^{-2}, I– 10^{-1}, J– 1; (a)–case 1; (b)–case 2; (c)–case 3.

Table 1. Incoming mass flux of the main chamber (kg/s)

Case	Fuel	Swirling primary air	First row primary air	Dilution and intermediate air
1	0.09	1.69	0	0
2	0.09	1.69	1.29	0
3	0.09	1.69	1.29	3.225

Our "numerical experiments" have been carried out to "measure" the flame structure variation due to the

937

change in the chamber parameters. The chamber structure parameters for each case are listed in table 1.

In the calculation the diffusion flame model (model B) is used. The fuel is taken to be propane (C_3H_8). The number of grids is 50x18x26 expanded into 3 MG level. The inlet fuel and air temperature is 300°K. Fig.2 shows the velocity vector field in the middle plane section in x–z plane as seen in figure 1. The different inlet arran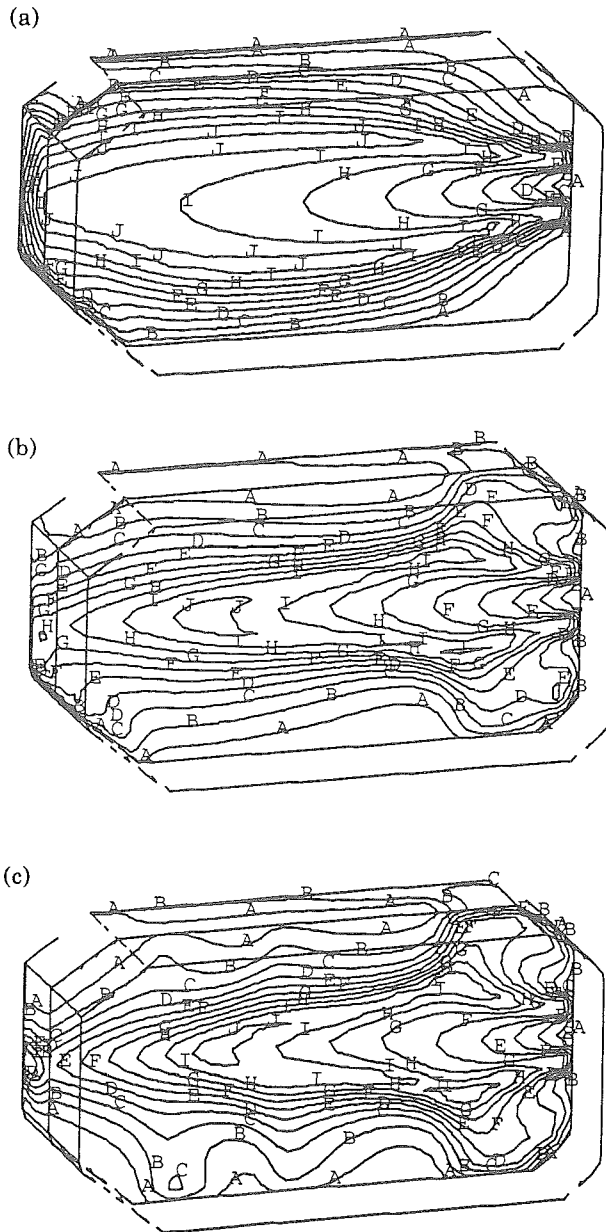gements result in extensive variation of the flow structure, cases 2 and 3 show better mixing of fuel and air than case 1. This is observed also in the fuel distribution field shown in figure 3 and temperature filed shown in figure 4. In figure 3 the location where the iso–fuel lines are dense is the flame sheet. One can find that in case 1, the flame is longer and wider so that the temperature at near wall regions changes fast. In this case the outlet temperature is uniformly as high as 2000°K. In case 2 and 3 the flame is shorter and narrower. The temperature of the upper and bottom walls is reduced by the introduction of dilution and intermediate air. The outlet temperature is 1000 – 1700 °K for case 2, and 700 – 1000 °K for case 3 respectively. This is beneficial for keeping the burner liner from overheating. In this way a suggestion that how much air should be supplied and where and at what direction may be found by numerical calculations.
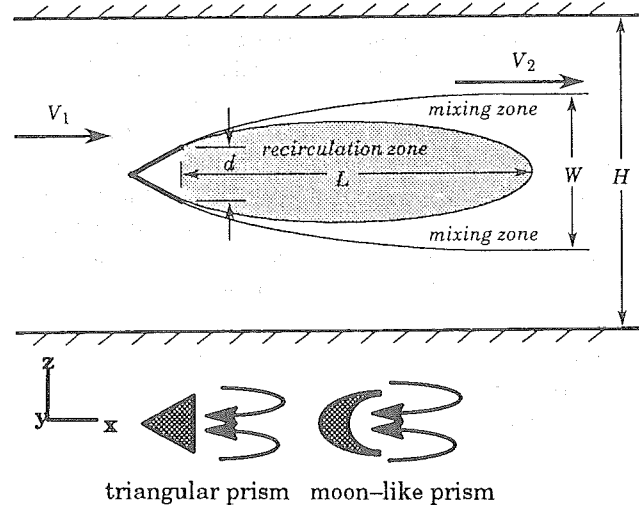
(a)

(b)

(c)

Figure 4. Calculated temperature field in the main chambers: A– 389, B– 582, C– 775, D–967, E– 1160, F–1353, G–1545, H–1738, I–1931, J–2123 (°K); (a)–case 1; (b)–case 2; (c)–case 3.

triangular prism   moon–like prism

Figure 5. Illustration of the afterburner and flame holder models
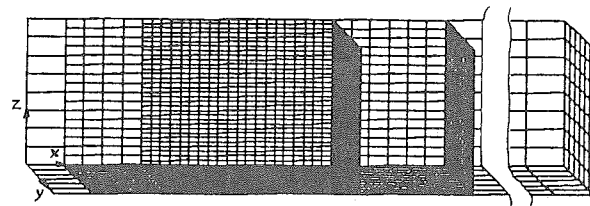
Figure 6. A sketch of grids used: the local grids are added around flame holders

4.2 The combustion in afterburners

Figure 5 shows an illustration of the afterburner of a gas turbine engine. The flame holder blockage ratio and shape are studied numerically. The running conditions are listed in table 2.

938

Table 2. Running conditions for the afterburner

Case	Flame holder shape	Blockage ratio
4	triangular prism	0.360
5	triangular prism	0.200
6	moon–like prism	0.333

The blockage ratio is defined as (blocked area)/(total area) in the cross section perpendicular to the incoming flow stream. The fuel used here is again propane. The incoming stream contains the exhausted gases from main burners and fresh fuel injected in the upstream of the afterburner. We assume that the fuel and air are fully mixed before the flame holder and the combustion is ignited in a location behind the flame holder. Therefore the finite reaction rate model (model A) is used. In the calculation 70x14x30 grids are used, which are expanded into 3 MG levels with one level of local grids 50x22x40 around flame holders. A typical grids sketch is shown in figure 6. The equivalent ratio of fuel is 0.6. Figure 7 shows the temperature field in the mid–plane parallel to the x–z plane as seen in figure 6. Figure 8 and 9 shows the carbon dioxide and unburned fuel fields in the same plane as in figure 6. In these figures, T_s, $\rho m_{co2,s}$, $\rho m_{fuel,s}$ are the computed values of temperature, carbon dioxide concentration and fuel concentrations close to the wall (where z/H=0.). η is defined as (distance in x– direction between inlet section and computed section) / (total length of the afterburner in x– direction). In figures 7–9, one vertical tic mark stands for 200°K difference in temperature, 1% difference in CO2 concentration, –0.5% difference in fuel concentration. The relevant values of T_s, $\rho m_{co2,s}$, $\rho m_{fuel,s}$ for various η are listed in table 3.

The reaction starts at η=0.25, the location immediately behind the flame holders. In case 6, the moon–like flame holder generates recirculation zones even for η<0.25 as illustrated in figure 5. The combustion started at η<0.25 for case 6 as seen in figures 7–9. In the calculations constant temperature (300 °K) is used as wall boundary conditions for the energy equation. The effect of flame holders can be illustrated clearly in these figures, with larger blockage ratio (case 4 and 6) the fuel consumption is more complete with higher temperature and stronger outlet gas stream. The relative values of the outlet gas momentum $(p+\rho U^2)$ is 1, 0.633, 0.983 for case 4, 5, and 6 respectively. Case 4 and 6 generate 36 percent larger forces compared to case 5.
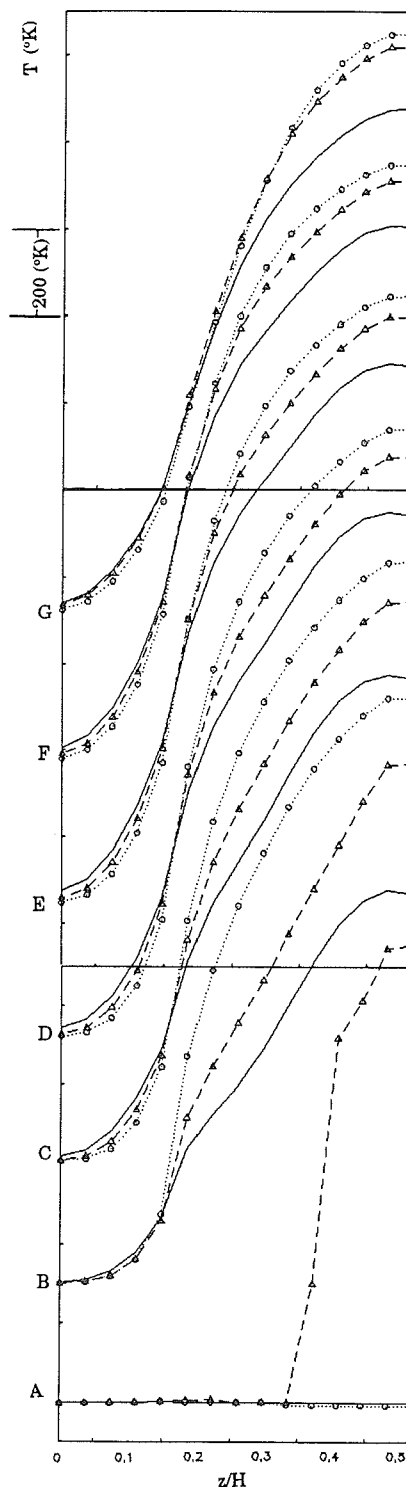

Figure 7. Calculated temperature field in the afterburners on the horizontal y– direction mid–width plane (x–z) (see figure 6), ⋯■⋯ case 4; —— case 5; –▲– case 6; each vertical line stands for 200 °K difference in temperature, detailed information is listed in table 3
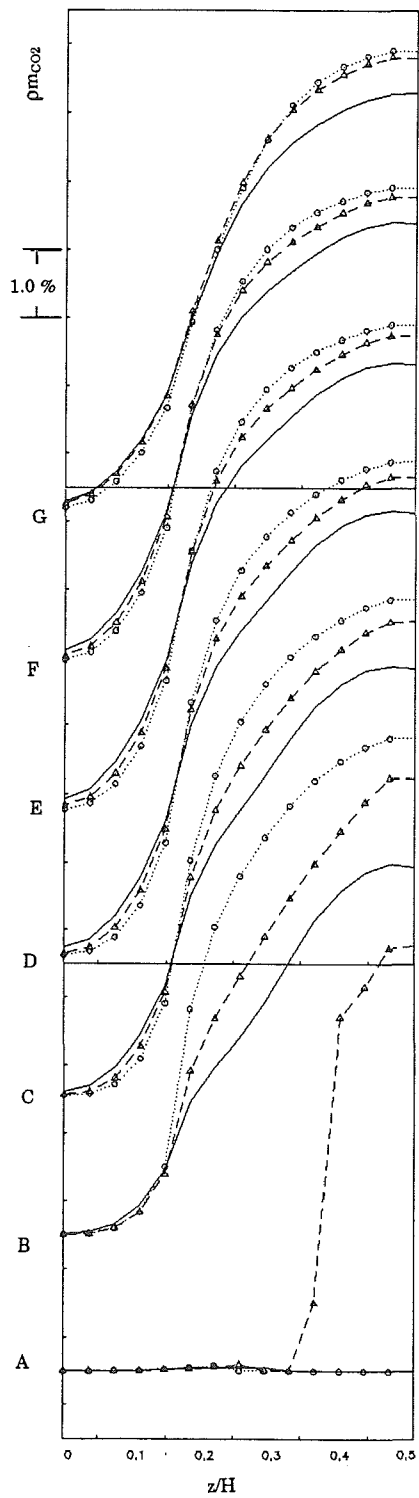
939

Figure 8. Calculated carbon dioxide field in the afterburners (the plotting plane and the legend as in figure 7)
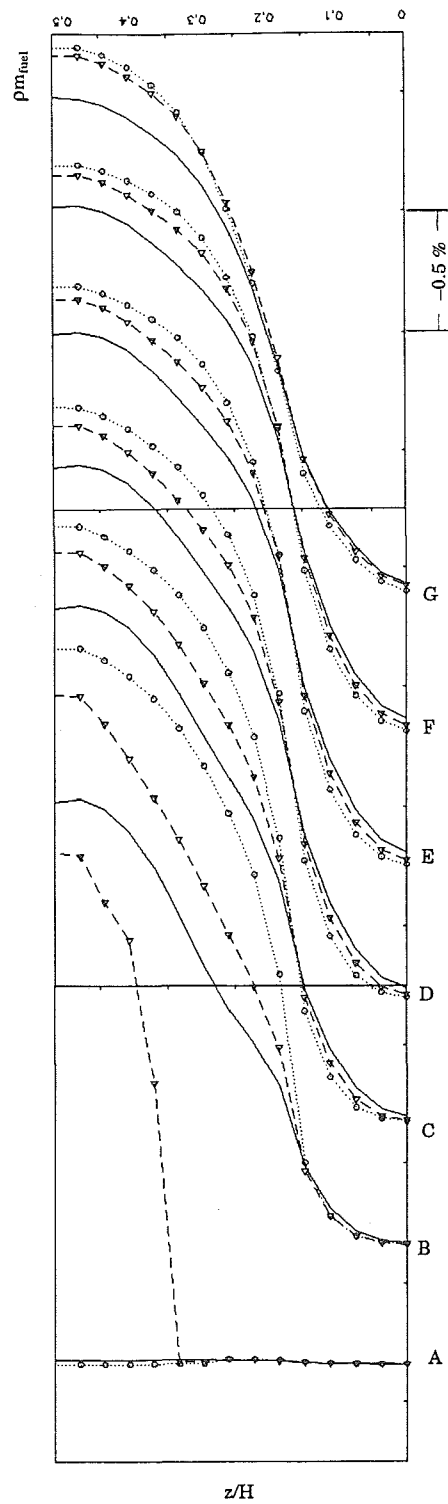
Figure 9. Calculated unburned fuel field in the afterburners (the plotting plane and the legend as in figure 7)

Table 3 Relevant values in figures 7–9

station	η	$\rho m_{co2,s}$ (%)	$\rho m_{fuel,s}$ (%)	T_s (°K)
A	0.25	0.001	2.59	300
B	0.375	0.014	2.58	300
C	0.5	0.052	2.57	307
D	0.625	0.131	2.54	322
E	0.75	0.283	2.49	349
F	0.875	0.453	2.43	380
G	1.0	0.698	2.35	423

5. Concluding Remarks

From the above examples, we may state that the mathematical models and numerical methods described in this paper can be applied to simulating turbulent reacting flows in the main combustion chambers and the afterburners of gas turbine engines with reasonable accuracy. The effect of fully air–fuel mixing and burning by introducing primary air through the first row of liner and the temperature–reducing effect of the dilution gases are captured in the calculations. In the after burner region the effect of flame holders blockage ratio and shape are well predicted. For flame stabilization sufficiently large blockage ratio is needed. In future researches we expect to include multi–step reaction schemes in the calculation. In that case the CO field can be calculated and hence the effect of intermediate air shown in figure 1 can be studied in greater detail.

Acknowledgement

References

[1] Williams F.A.: "Turbulent Combustion", The Mathematics of Combustion, Chapter 3, J.D. Buckmaster eds., SIAM Philadelphia, 1985.

[2] Speziale, C.G.: "Discussion of Turbulence Modeling: Past and Future", NASA CR 181884, 1989.

[3] Launder, B.E. and Spalding, D.B.:" The Numerical Computation of Turbulent Flows", Computer Methods in Applied Mechanics and Engineering, Vol.3, 1974, pp.269–289.

[4] Rodi, W.: "Turbulence Models and Their Application in Hydaulics – A State of The Art Review", Institut for Hydromechanik, 1980.

[5] Pope, S.B.: "Turbulent Premixed Flames", Ann. Rev. Fluid Mechanics, No.19, 1987.

[6] Borghi, R.: "Turbulent Combustion Modelling ", Progress in Energy and Combustion Science, Vol. 14, 1989.

[7] Magnussen, B.F. and Hjertager, B.H.: "On Mathematical Modelling of Turbulent Combustion with Special Emphasis on Soot Formation and Combustion", 16th Symposium (Int.) on Combustion, The Combustion Institute, pp. 719–729, 1976.

[8] Jone, W.P. and Whitelaw, J.H.: "Calculation Methods for Reacting Turbulent Flows: A Review", Combustion Science and Technology, Vol. 48, pp.1–26, 1982.

[9] Jennings, M.J. and Morel, T.: "Obeservations on the Application of the k–e Model to Internal Combustion Engine Flows", Combustion Science and Technology, Vol. 58, pp.177–193, 1988.

[10] Bai, X.S. and Fuchs, L.: "Numerical Simulation of Windtunnel Flows Past a Flame Holder Model", Proc. of 9–th GAMM Conference on Computational Fluid Dynamics, Swizerland, Sept. 1991.

[11] Hutchinson, P.; Khalil, E.E. and Whitelaw, J. H.: "Measurement and Calculation of Furnace Flow Properties", J. of Energy, Vol.1, No.4, 1977.

[12] Khalil, E.E. : **Modelling of Furnaces and Combustors**, ABACUS Press, 1982.

[13] Bai, X.S. and Fuchs, L.: "Numerical Simulations of Flows Around Flame Holders", AIAA Paper 92–0557, 1992.

[14] Bai, X.S. and Fuchs, L.:"A Fast Multi–Grid Method for 3–D Turbulent Incompressible Flows", Int. J. of Numer. Method for Heat and Fluid Flows, Vol. 2 ,1992.

[15] Fuchs, L.:"A Local Mesh Refinement Technique For Incompressible Flows", Computers & Fluids, Vol. 14, No.1, 1986, pp.69–81.